Fragmentation of heme and hemin+ with sequential loss of carboxymethyl groups: A DFT and mass–spectrometry study

ARTICLE *in* CHEMICAL PHYSICS LETTERS · NOVEMBER 2005

Impact Factor: 1.9 · DOI: 10.1016/j.cplett.2005.09.036

9 AUTHORS, INCLUDING:

Oleg. Petrovich Charkin
Russian Academy of Sciences
240 PUBLICATIONS **1,050** CITATIONS

SEE PROFILE

Available online at www.sciencedirect.com
SCIENCE DIRECT®
Chemical Physics Letters 415 (2005) 362–369
CHEMICAL PHYSICS LETTERS
www.elsevier.com/locate/cplett

Fragmentation of heme and hemin$^+$ with sequential loss of carboxymethyl groups: A DFT and mass-spectrometry study

O.P. Charkin [a,b,*], N.M. Klimenko [a,c], P.T. Nguyen [a], D.O. Charkin [d], A.M. Mebel [e], S.H. Lin [a], Y.-S. Wang [a], S.-C. Wei [a], H.-C. Chang [a]

[a] *Institute of Atomic and Molecular Sciences, Academia Sinica, Taipei 106, Taiwan*
[b] *Institute of Problems of Chemical Physics, Russian Academy of Sciences, Chernogolovka, Moscow Region 142432, Russia*
[c] *Lomonosov's Moscow State Academy of Fine Chemical Technology, Moscow 117571, Russia*
[d] *Department of Material Sciences, Lomonosov's Moscow State University, Moscow 119992, Russia*
[e] *Florida International University, Department of Chemistry and Biochemistry, Miami, FL 33199, USA*

Received 13 July 2005; in final form 7 September 2005
Available online 3 October 2005

Abstract

Density functional B3LYP calculations with the 6-31G* and mixed 6-31G* (Fe) + 6-31G (C, H, N, O) basis sets have been performed to study the electronic and geometric structure, thermodynamic stability, and vibrational frequencies of the heme molecule $FeC_{34}H_{32}N_4O_4$, its ion $FeC_{34}H_{32}N_4O_4^+$, and products of their fragmentation with sequential elimination of two carboxymethyl groups in the electronic states with different spin multiplicities. The fragmentation energies were refined with the larger 6-311++G** basis set. Results of the calculations are compared with available experimental data. The trends in the aforementioned properties with a change of the multiplicity, molecular charge, and the number of external carboxymethyl ligands present have been analyzed.

1. Introduction

Biological functions of metalloporphyrins (MPs) encompass a wide variety from oxygen storage and transport to electron transport and energy conversion [1]. MPs themselves possess intriguing photosensitizing and catalytic properties [2], and they remain to be a focus of numerous spectroscopic studies, mostly in condensed phases, where the chemical behavior and reactivity of MPs are strongly influenced by solvent. To study MPs without solvent interference, the molecules can be transferred from a condensed phase into the gas phase as isolated free ions by using electrospray ionization and mass-spectrometric registration of the ions [3].

Responsible for the transport and storage of oxygen in biological circulation systems, heme is a prosthetic group bound to the polypeptide chains of hemoproteins, such as myoglobin [4]. It contains a protoporphyrin ring with either Fe(II) or Fe(III) in the center, and two propionate (Pr), four methyl (Me) and two vinyl (Vi) peripheral groups (structure **1** in Fig. 1). Mechanisms of the heme reactions with O_2, CO, NO, CN^-, and other biologically active ligands continue to be an important topic of numerous experimental and theoretical investigations [1,2,5–11].

The present communication is devoted to a combined theoretical and experimental study of fragmentation of the isolated heme (i.e., $Fe(II)C_{34}H_{32}N_4O_4$) molecule and its positive ion, hemin$^+$ (i.e., $Fe(III)C_{34}H_{32}N_4O_4^+$), with sequential loss of two carboxymethyl (CMe) groups. The Letter consists of two parts and includes: (1) density functional B3LYP calculations of the geometric and electronic structure, energetics, and vibrational frequencies of heme, hemin$^+$, and the products of their fragmentation in the states of various spin multiplicities; (2) experimental study of

* Corresponding author. Fax: +7 096 517 8910.
E-mail addresses: charkin@icp.ac.ru (O.P. Charkin), mebela@fiu.edu (A.M. Mebel), wer@gate.sinica.edu.tw (Y.-S. Wang), hcchang@po.iams.sinica.edu.tw (H.-C. Chang).

0009-2614/$ - see front matter © 2005 Elsevier B.V. All rights reserved.
doi:10.1016/j.cplett.2005.09.036

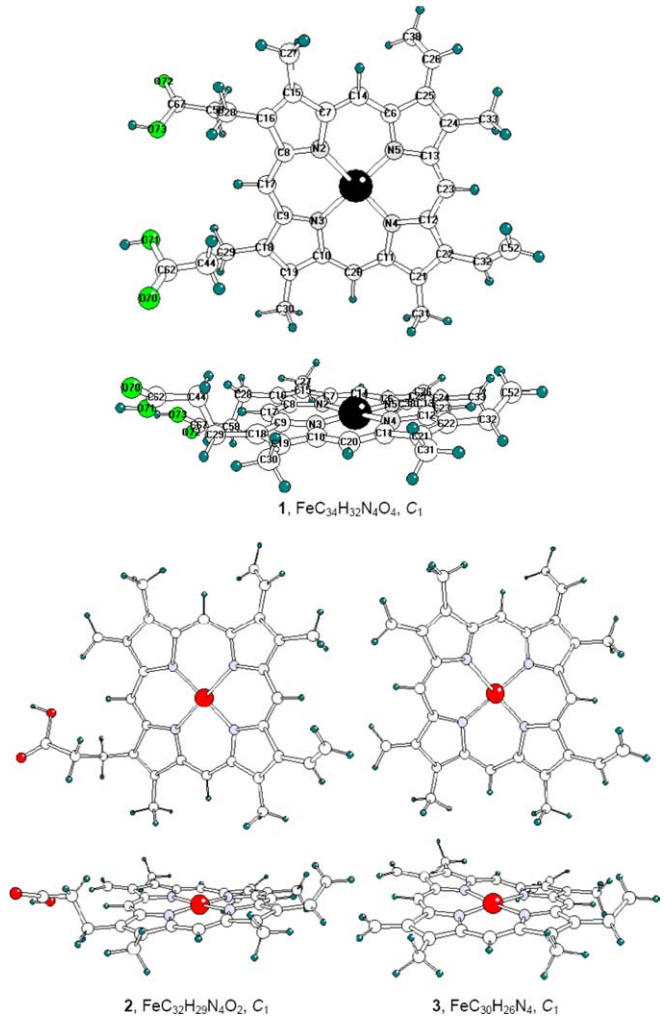

Fig. 1. Structures of heme (**1**), either neutral or positively charged, and their fragmentation products (**2**, **3**) after sequential loss of two carboxymethyl groups. In structure **1**, the Fe ion (either Fe(II) or Fe(III)) is marked in black and the N, C, O and H atoms are denoted by gray, white, light green and dark green spheres, respectively. (For interpretation of the references to color in this figure legend, the reader is referred to the web version of this article.)

hemin$^+$ fragmentation by either photodissociation or collision-induced dissociation in an ion cyclotron resonance cell. The goal of the Letter is to calculate the equilibrium geometry and relative energies of low-, middle- and high-spin states of the above mentioned molecules, and to evaluate the consecutive bond energies $D_i^0(\mathrm{CMe})$ and $D_i^+(\mathrm{CMe})$ ($i = 1$ and 2) corresponding to the following reactions

$$\mathrm{FeC_{34}H_{32}N_4O_4}\ (\mathbf{1}) \rightarrow \mathrm{FeC_{32}H_{29}N_4O_2}\ (\mathbf{2}) + \mathrm{CH_2COOH} + D_1^0(\mathrm{CMe}) \quad (1)$$

$$\mathrm{FeC_{32}H_{29}N_4O_2}\ (\mathbf{2}) \rightarrow \mathrm{FeC_{30}H_{26}N_4}\ (\mathbf{3}) + \mathrm{CH_2COOH} + D_2^0(\mathrm{CMe}) \quad (2)$$

$$\mathrm{FeC_{34}H_{32}N_4O_4^+}\ (\mathbf{1}^+) \rightarrow \mathrm{FeC_{32}H_{29}N_4O_2^+}\ (\mathbf{2}^+) + \mathrm{CH_2COOH} + D_1^+(\mathrm{CMe}) \quad (3)$$

$$\mathrm{FeC_{32}H_{29}N_4O_2^+}\ (\mathbf{2}^+) \rightarrow \mathrm{FeC_{30}H_{26}N_4^+}\ (\mathbf{3}^+) + \mathrm{CH_2COOH} + D_2^+(\mathrm{CMe}) \quad (4)$$

and to analyze the relations between the multiplicity and geometry of heme, hemin$^+$, and their decay products. The study is a crucial step toward our detailed elucidation for the mechanism of heme dissociation from the myoglobin pocket [12].

Fragmentation of hemin$^+$ has been studied earlier experimentally in [5], where the first bond energy $D_1^+(\mathrm{CMe}) < 2.5 \pm 0.3$ eV was measured, and the second bond energy $D_2^+(\mathrm{CMe})$ was evaluated to be very low, $D_1^+(\mathrm{CMe}) \gg D_2^+(\mathrm{CMe})$. The latter result seems quite unusual. The authors explained it as result of the delocalization of an unpaired electron in the π-electron network of the porphyrin ring, although the electronic and geometric structure, multiplicity, and other characteristics of the hemin$^+$ ion and its fragmentation products in [5] were not addressed.

2. Computational and experimental detail

All calculations have been carried out within the hybrid DFT B3LYP method [13], combining Becke's 3-parameter exchange functional [14] with the correlation functional by Lee, Yang, and Parr [15], with various basis sets and using the GAUSSIAN-03 program [16]. The accuracy of geometry optimization and calculations of normal vibrational frequencies for middle- and high-spin states of heme and hemin$^+$ was tested by employing two basis sets, the standard 6-31G* and a more economical mixed basis set 6-31G* (Fe) + 6-31G (C, H, N, O) denoted below as Gen. In the latter, the polarization functions (*f* functions in this case) were included on Fe atom only. A comparison of the results computed with these two basis sets demonstrated that the economical Gen basis set reduces the computational time and the required computer facilities by several times without a tangible loss in accuracy of calculated geometry parameters, vibrational frequencies, and electron density distribution as compared to the standard 6-31G*. In particular, the geometry is reproduced almost identically, and the differences in most vibrational frequencies vary within 5–15 $\mathrm{cm^{-1}}$ and do not exceed 30 $\mathrm{cm^{-1}}$. Hence, the geometry optimization and calculations of vibrational frequencies of all species in Eqs. (1)–(4) with various multiplicities have been performed at the B3LYP/Gen level. Their energetic parameters were finally determined more precisely by single-point calculations at our highest B3LYP/6-311++G**//B3LYP/Gen level of theory.

Structures **1**–**3** are depicted in Fig. 1. Table 1 summarizes total E_{tot} and relative E_{rel} energies of structures **1**–**3** with various spin multiplicities, their zero-point energies (ZPE) as well as calculated effective charges Z(Fe) and spin densities ρ(Fe) on the Fe atom. Calculated bond energies $D_i^0(\mathrm{CMe})$ and $D_i^+(\mathrm{CMe})$ are compared with results of their experimental data in Table 2. Selected geometric parameters of the porphyrin ring in the structures **1**–**3** are presented in Table 3. We will focus mostly on relative changes in molecular characteristics with a change of

Table 1
Total (E_{tot}) and relative (E_{rel}) energies of electronic states with different multiplicities, effective charge Z(Fe) and spin density ρ(Fe) on the Fe atom in heme, hemin$^+$, and products of their decomposition[a]

Species	Multiplicity	E_{tot} (a.u.)	ZPE[b] (kcal/mol)	E_{rel} (eV)[c]	Z(Fe) (e)	ρ(Fe)[d] (e)
$FeC_{34}H_{32}N_4O_4$ (**1**)	Singlet	−3099.07360		1.45	+0.93	
	Triplet	−3099.12725	376.7	0.0	+0.99	2.00
	Quintet	−3099.11881	375.2	0.17	+1.02	3.74
$FeC_{34}H_{32}N_4O_4^+$ (**1**$^+$)	Doublet	−3098.87188	377.0	0.51	+0.94	1.99
	Quartet	−3098.89049	377.0	0.0	+1.28	2.95
	Sextet	−3098.81290	374.8	2.01	+1.14	3.86
$FeC_{32}H_{29}N_4O_2$ (**2**)	Doublet	−2870.53040	340.9	0.0	+0.91	1.98
	Quartet	−2870.31907	342.4	0.07	+0.91	2.00
	Sextet	−2870.31039	341.2	0.20	+1.03	3.75
$FeC_{32}H_{29}N_4O_2^+$ (**2**$^+$)	Singlet	−2870.26201		1.57	+1.00	
	Triplet	−2870.31907	342.4	0.0	+0.94	1.98
	Quintet	−2870.31039	341.2	0.19	+1.07	3.74
$FeC_{30}H_{26}N_4$ (**3**)	Singlet	−2641.87991	306.6	1.45	+0.90	
	Triplet	−2641.93329	306.6	0.0	+0.90	1.98
	Quintet	−2641.92619	304.6	0.10	+0.92	2.03
	Septet	−2641.91994	303.3	0.22	+1.04	3.75
$FeC_{30}H_{26}N_4^+$ (**3**$^+$)	Doublet	−2641.70147	306.7	0.58	+0.95	1.95
	Quartet	−2641.72279	306.7	0.0	+1.16	2.48
	Sextet	−2641.67874	304.9	1.10	+1.07	3.75

[a] Calculated at the B3LYP/6-311+G**//B3LYP/Gen + ZPE(B3LYP/Gen) level. The total energy and ZPE of carboxymethyl radical CH_2COOH calculated at the same level of theory are −228.49878 a.u. and 30.1 kcal/mol, respectively.
[b] Zero-point vibrational energies (ZPE).
[c] Relative energies of various electronic states with respect to the ground state, i.e., with respect to the multiplet with the lowest energy.
[d] Spin density on the Fe atom (in units of e).

multiplicity, molecular charge, and the number of external carboxymethyl (CMe) groups.

Experimental measurements were conducted using a 7 T Fourier transform ion cyclotron resonance (FT-ICR) mass spectrometer (Apex IV, Bruker Daltonics) equipped with an external electrospray ionization (ESI) source. The sample solution consisted of 5 μM myoglobin prepared in 15% methanol containing 2% formic acid with pH < 3. At this pH range, myoglobin denatured and the heme group was detached from the protein pocket [17]. The heme$^+$ ions were generated by ESI of the denatured protein solution, accumulated in a hexapole ion trap located in the fringe field region, and pulsed into the ICR cell. Mono-isotopic hemin$^+$ ions were isolated from the ion packet using an RF clean-up sweep and then excited with a cw diode laser (BCL-405-050, CrystaLaser) at the wavelength of 405 nm, corresponding to the Soret absorption band of porphyrin [17]. A computer-controlled mechanical shutter chopped the laser beam and the photofragmentation events were recorded and subsequently analyzed. Fig. 2 depicts the fragmentation pattern of hemin$^+$ in the ICR cell with different laser duration.

The dissociation energies D_1^+ and D_2^+ were measured with an on-resonance RF excitation and collision-induced dissociation (CID) method. Detailed descriptions of the method will be presented in [12]. Briefly, the hemin$^+$ ion after isolation and collision cooling in the ICR cell was excited translationally at its resonance frequency using amplitude-fixed RF pulses. The resulting translational energy (E_{tr}) in the laboratory frame was deduced mathematically according to the RF frequency, amplitude, excitation duration, cell shape, cell dimension, and the molecular weight of the ion investigated [18]. The excited ions were then collided with pulsed Ar gas, and the dissociation threshold was finally determined from a curve plotted in terms of dissociation fraction versus center-of-mass energy, E_{CM} =

Table 2
Dissociation energies D_i(CIe) for sequential elimination of carboxymethyl groups H_2CCOOH from heme and hemin$^+$ calculated at the B3LYP level with the Gen, 6-31G*, and 6-311++G** basis sets (in eV)[a]

Reactions	Gen	6-31G*	6-311++G**	Experiment
$FeC_{34}H_{32}N_4O_4$ (**1**) → $FeC_{32}H_{29}N_4O_2$ (**2**) + H_2CCOOH − D_1^0	2.72 (2.45)	2.97 (2.70)	2.97 (2.70)	
$FeC_{32}H_{29}N_4O_2$ (**2**) → $FeC_{30}H_{26}N_4$ (**3**) + H_2CCOOH − D_2^0	2.82 (2.64)	2.87 (2.69)	2.67 (2.49)	
$FeC_{34}H_{32}N_4O_4^+$ (**1**$^+$) → $FeC_{32}H_{29}N_4O_2^+$ (**2**$^+$) + H_2CCOOH − D_1^+	2.38 (2.20)	1.94 (1.76)	1.98 (1.80)	$\leqslant 2.5 \pm 0.3$ [5] 1.9 ± 0.2 (This work)
$FeC_{32}H_{29}N_4O_2^+$ (**2**$^+$) → $FeC_{30}H_{26}N_4^+$ (**3**$^+$) + H_2CCOOH − D_2^+	2.55 (2.31)	2.71 (2.47)	2.65 (2.41)	$\ll D_1$ [5] 2.4 ± 0.3 (This work)

[a] Calculated at the geometries optimized at the B3LYP/Gen level. The D_i(CIe) values given without and in parentheses are computed, respectively, without and with ZPE(B3LYP/Gen) taken into account.

Table 3
Optimized interatomic distance $R(i-j)$ in heme, hemin$^+$, and their fragmentation products in electronic states of different multiplicities (in Å)[a]

	Fe–N	N_2–C_7	N_2–C_8	C_7–C_{14}	C_7–C_{15}	C_8–C_{16}	C_8–C_{17}	C_{15}–C_{16}	C_{15}–C_{27}	C_{16}–C_{28}	C_{28}–C_{58}
Species, structure, multiplicity											
$FeC_{34}H_{32}N_4O_4$ (**1**)											
Singlet	1.970	1.392	1.391	1.384	1.452	1.454	1.386	1.376	1.499	1.502	1.567
Triplet	1.995	1.392	1.391	1.384	1.452	1.455	1.386	1.376	1.499	1.502	1.557
Quintet	2.058	1.387	1.386	1.395	1.460	1.460	1.397	1.379	1.500	1.502	1.558
$FeC_{34}H_{32}N_4O_4^+$ (**1**$^+$)											
Doublet	1.990	1.372	1.407	1.404	1.462	1.464	1.370	1.372	1.497	1.503	1.562
Quartet	1.956	1.404	1.404	1.380	1.441	1.443	1.392	1.387	1.498	1.501	1.555
Sextet	2.049	1.373	1.401	1.411	1.464	1.468	1.381	1.376	1.498	1.501	1.555
$FeC_{32}H_{29}N_4O_2$ (**2**)											
Doublet	1.955	1.412	1.382	1.393	1.422	1.477	1.379	1.425	1.495	1.378	–
Quartet	1.999	1.408	1.380	1.389	1.430	1.476	1.382	1.419	1.495	1.384	–
Sextet	2.062	1.403	1.375	1.400	1.434	1.482	1.392	1.426	1.495	1.381	–
$FeC_{32}H_{29}N_4O_2^+$ (**2**$^+$)											
Singlet	1.974	1.439	1.364	1.405	1.391	1.481	1.385	1.449	1.492	1.353	–
Triplet	1.990	1.434	1.359	1.409	1.390	1.483	1.390	1.452	1.492	1.353	–
Quintet	2.058	1.430	1.353	1.421	1.394	1.489	1.403	1.459	1.492	1.352	–
$FeC_{30}H_{26}N_4$ (**3**)											
Singlet	1.956	1.440	1.387	1.411	1.384	1.481	1.373	1.449	1.495	1.356	–
Triplet	1.997	1.438	1.367	1.409	1.389	1.490	1.382	1.445	1.495	1.357	–
Quintet	2.000	1.409	1.379	1.383	1.436	1.475	1.383	1.415	1.495	1.386	–
Septet	2.066	1.404	1.374	1.394	1.440	1.482	1.393	1.422	1.494	1.384	–
$FeC_{30}H_{26}N_4^+$ (**3**$^+$)											
Doublet	1.990	1.430	1.367	1.401	1.401	1.486	1.382	1.443	1.492	1.357	–
Quartet	1.975	1.438	1.371	1.405	1.392	1.484	1.381	1.446	1.493	1.357	–
Sextet	2.064	1.423	1.361	1.410	1.408	1.492	1.394	1.449	1.492	1.357	–
$(FeC_{34}H_{31}N_4O_4)_2$, C_i dimer, experiment [19]		1.379	1.411	1.374	1.435	1.436	1.382	1.347	1.513	1.575	1.58
	N_5–C_6	N_5–C_{13}	C_6–C_{25}	C_6–C_{14}	C_{13}–C_{23}	C_{13}–C_{24}	C_{24}–C_{25}	C_{24}–C_{33}	C_{25}–C_{26}	C_{26}–C_{38}	C_{58}–C_{67}
Species, structure, multiplicity											
$FeC_{34}H_{32}N_4O_4$ (**1**)											
Singlet	1.393	1.401	1.443	1.382	1.382	1.443	1.382	1.499	1.460	1.342	1.504
Triplet	1.390	1.393	1.459	1.385	1.386	1.446	1.383	1.499	1.462	1.346	1.504
Quintet	1.384	1.388	1.465	1.396	1.396	1.452	1.386	1.499	1.462	1.346	1.503
$FeC_{34}H_{32}N_4O_4^+$ (**1**$^+$)											
Doublet	1.404	1.377	1.471	1.372	1.406	1.451	1.381	1.498	1.458	1.347	1.506
Quartet	1.403	1.405	1.447	1.381	1.382	1.436	1.389	1.498	1.461	1.347	1.508
Sextet	1.398	1.377	1.474	1.381	1.413	1.455	1.384	1.498	1.459	1.347	1.508
$FeC_{32}H_{29}N_4O_2$ (**2**)											
Doublet	1.394	1.392	1.462	1.379	1.384	1.448	1.380	1.499	1.462	1.346	–
Quartet	1.390	1.392	1.460	1.384	1.386	1.446	1.382	1.499	1.462	1.346	–
Sextet	1.386	1.388	1.466	1.394	1.396	1.452	1.386	1.499	1.462	1.346	–
$FeC_{32}H_{29}N_4O_2^+$ (**2**$^+$)											
Singlet	1.413	1.387	1.459	1.363	1.399	1.440	1.389	1.498	1.459	1.347	–
Triplet	1.411	1.374	1.466	1.364	1.403	1.453	1.378	1.498	1.461	1.346	–
Quintet	1.405	1.370	1.472	1.374	1.414	1.458	1.381	1.498	1.462	1.346	–
$FeC_{30}H_{26}N_4$ (**3**)											
Singlet	1.414	1.377	1.472	1.359	1.390	1.460	1.373	1.497	1.458	1.347	–
Triplet	1.407	1.380	1.470	1.365	1.388	1.458	1.374	1.498	1.462	1.346	–
Quintet	1.388	1.396	1.457	1.389	1.386	1.442	1.385	1.499	1.461	1.346	–
Septet	1.383	1.390	1.463	1.399	1.396	1.448	1.388	1.499	1.462	1.346	–
$FeC_{30}H_{26}N_4^+$ (**3**$^+$)											
Doublet	1.402	1.385	1.468	1.369	1.388	1.455	1.375	1.497	1.461	1.346	–
Quartet	1.411	1.389	1.467	1.364	1.386	1.453	1.375	1.497	1.461	1.346	–
Sextet	1.393	1.379	1.473	1.384	1.401	1.461	1.380	1.497	1.462	1.345	–
$(FeC_{34}H_{31}N_4O_4)_2$, C_i dimer, experiment [19]	1.360	1.388	1.451	1.403	1.370	1.461	1.339	1.551	1.527	1.31	1.50

[a] Calculated at the B3LYP/Gen level. Interatomic distances are given for the upper half of the P-ring. Bond lengths in the lower half of the P-ring do not deviate from their upper analogs by more than few hundredths of an angstrom.

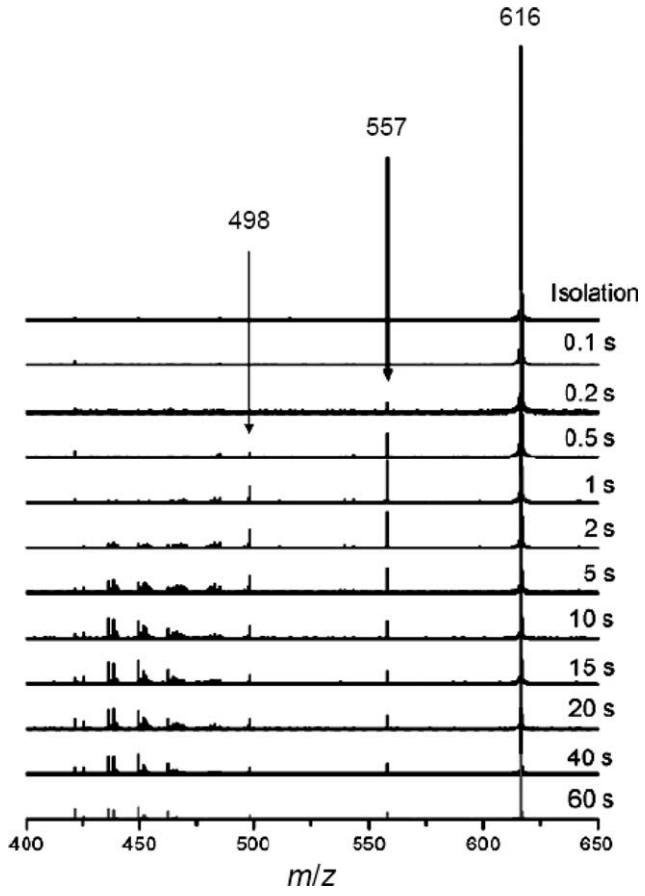

Fig. 2. Change of the photofragmentation pattern of isolated hemin$^+$ as a function of laser excitation time. The excitation was conducted at $\lambda = 405$ nm from a cw diode laser. The peaks denoted at m/z 557 and 498 correspond to [heme–CH_2COOH]$^+$ and [heme–$(CH_2COOH)_2$]$^+$ ions, respectively.

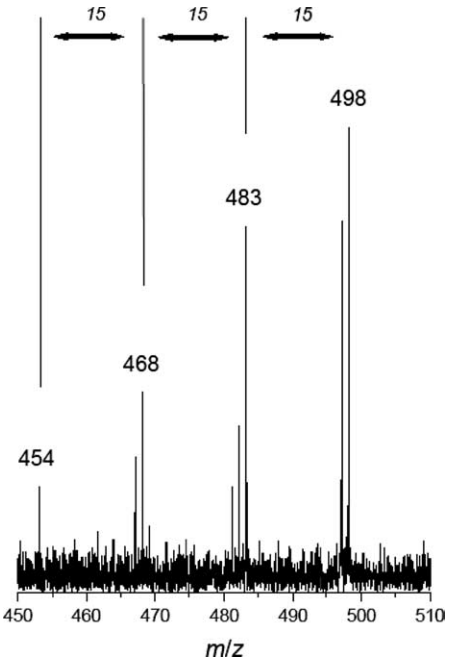

Fig. 3. Collision-induced dissociation pattern of the isolated [heme–CH_2COOH]$^+$ ion (m/z 557). Note the significant reduction of the CID products, as compared to the photofragmentation products shown in Fig. 2. Further fragmentation of the product ion [heme–$(CH_2COOH)_2$]$^+$ leads to sequential loss of methyl groups (m/z 15). The peaks separated by 1 amu for each fragment correspond to isotopic species.

$m_{Ar}E_{tr}/(m_{heme^+} + m_{Ar})$, where m_{heme^+} and m_{Ar} are the masses of Ar and heme$^+$, respectively [12]. Further measurement of the dissociation threshold of the second side chain group on heme$^+$ was conducted by isolating the [heme–CH_2COOH]$^+$ fragment for collision with Ar atoms in the ICR cell. Fig. 3 shows the CID fragment pattern of the isolated [heme–CH_2COOH]$^+$. The CID dissociation fractions of the parent ions versus E_{CM} for these two fragmentation processes are plotted in Fig. 4, corresponding to the loss of the first and second carboxymethyl groups as described by Eqs. (3) and (4), respectively.

3. Results and discussion

3.1. Heme and hemin$^+$ structures

All calculated systems with structures **1**–**3**, both neutral and positively charged, with low, middle, and high spins, have only real vibration frequencies, and each of the states under discussion corresponds to a true local minimum on the potential energy surface (PES). In all these minima, the Fe atom, like in the Fe(II)–porphyrin, is located very close to the center of the NNNN 'core'. (Strictly speaking, due to a low symmetry (C_1), Fe is shifted from the center and out of the NNNN plane by a few hundredths of Å, but these shifts seem to be too minor and probably do not (or only slightly) exceed a computational error and therefore are not discussed here.)

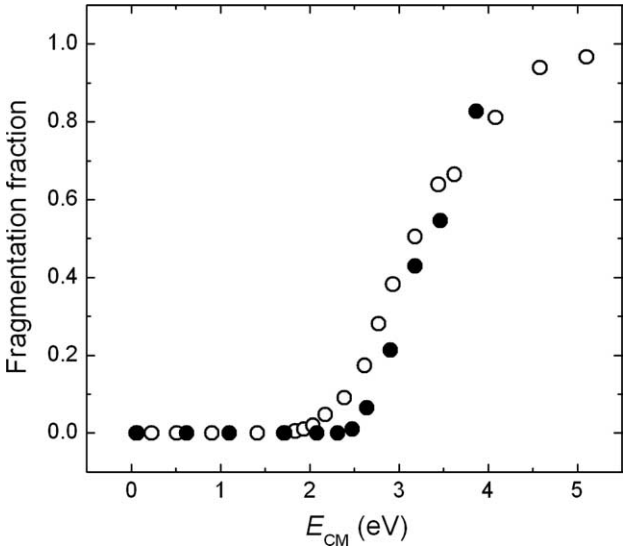

Fig. 4. Collision-induced dissociation fractions versus collision energies (expressed in terms of E_{CM}) for the two fragmentation processes described in Eqs. (3) and (4) in the text, i.e., the loss of the first (○) and second (●) carboxymethyl groups of hemin$^+$. The fragmentation fraction is defined as $I_{616}/(I_{616} + I_{557})$ for (○) and $I_{557}/(I_{557} + I_{498})$ for (●), where I is the abundance of the ion with the specified m/z value in the ICR cell.

As one can see in Table 1, the ground state of heme $FeC_{34}H_{32}N_4O_4$ (**1**) is calculated to be triplet with two unpaired electrons localized on the Fe atom (spin-density $\rho(Fe) = 2.00$, here and below given in fractions of an electron). The nearest quintet with four unpaired electrons on Fe (with $\rho(Fe) = 3.74$) is very close and lies only ~0.2 eV above, while the nearest singlet state is significantly (by ~1.5 eV) less favorable as compared to the lowest triplet. This result is in accord with previous experimental and theoretical data for the symmetrical non-substituted Fe(II)–porphyrin $FeC_{20}H_{12}N_4$ (D_{4h}) (see [8,9] and references therein), which also has a triplet ground state $^3A_{2g}$, a quintet $^5A_{1g}$ state and a singlet $^1A_{1g}$ state lying by ~0.3 and ~1.35 eV higher in energy, respectively, indicating that the low symmetry and external substituents of the heme molecule do not significantly affect the relative energetic order of the lowest singlet, triplet, and quintet states.

The calculated lowest state of the hemin$^+$ ion, $FeC_{34}H_{32}N_4O_4^+$ (**1**), is quartet with three unpaired electron on the Fe atom ($\rho(Fe) = 2.95$). The nearest sextet with four unpaired electron on Fe ($\rho(Fe) = 3.86$) and with one spin delocalized on the porphyrin ring (below P-ring) is energetically unfavorable, ~2.0 eV above the quartet state. In the lowest doublet, which lies by ~0.5 eV above the quartet, the Fe atom has two parallel spins ($\rho(Fe) = 1.99$) and one spin delocalized in the P-ring is opposite. Upon heme ionization, an electron is detached from the central Fe atom. The calculated adiabatic ionization potential of heme is 6.45 eV after taking ZPE corrections into account.

The analysis of optimized geometric parameters indicates that the lengths of bonds like C_{29}–C_{44} (~1.55 Å), C_{15}–C_{27} (~1.50 Å), and C_{25}–C_{26} (~1.46 Å), which respectively connect the external carboxymethyl, methyl, and vinyl groups with the P-ring, are shortened (and these bonds are conversely strengthened) in the row of CMe > Me > Vi, both in heme and in hemin$^+$. This trend is in a qualitative agreement with time-resolved mass-spectra of hemin$^+$ (Fig. 2). The major fragments in the first second are the ions with m/z 557 and 498, corresponding to the losses of the first and second carboxymethyl groups. Elongating the excitation duration results in the production of complex fragments that can be grouped into four bands populated at m/z 485–475, 470–463, 456–449, and 440–435, corresponding to combinations of bond cleavages in other side chain groups. Carboxymethyl groups are cleaved first, followed by cleavage of four methyl groups, and the rest two vinyl groups are bound to the P-ring most strongly.

To our best knowledge, no experimental data are available on equilibrium geometry of the isolated heme molecule and hemin$^+$ ion. It is worth to compare our calculated geometric parameters with results of the X-ray study of crystal (powder) structure of β-heamatin, $(Fe(III)C_{34}H_{30}N_4O_4)_2$, C_i [19]. Note that this comparison is not completely warranted and cannot be quantitative because of numerous additional effects, which influence the crystal structure, such as dimerization via two Fe–O–C bridge bonds between P-rings and a strong shift of the Fe atoms perpendicular to the NNNN planes, two hydrogen bonds and other long-range interactions between neighboring dimers, large-amplitude vibrations or rotation of external groups around single C–C bonds, packing effects, the temperature factor, etc., but are not present in the isolated heme molecule. Hence, we limit ourselves to a comparison of geometric parameters only for the relatively 'rigid' porphyrin ring, in belief that the influence of aforementioned factors on the P-ring parameters should be minimal. As seen in Table 2, the calculated and measured internuclear distances in the P-ring of the free heme molecule and crystal β-heamatin are in reasonable semi-quantitative agreement with each other. Differences mostly lie in narrow margins of 0.02–0.03 Å with exception of the 'outer' bonds in the pyrrole cycles, which are shorter by 0.03–0.05 Å in β-heamatin as compared to those in the heme. Bond length alteration in β-heamatin is manifested slightly more clearly, but the differences do not exceed few hundredths of Å either. Also, the calculated average values of the R(Fe–N) distances for the triplet (1.995 Å) and quintet (2.058 Å) states of heme (**1**) are close to the corresponding experimental values of 1.972 and 2.057 Å for triplet Fe(II)(TPP), $^3A_{2g}$ [20], and quintet Fe(II)(TPP)(THF), $^5A_{1g}$ [21], respectively (TPP, tetraphenylporphyrin; THF, tetrahydrofuran).

Internuclear distances and bond angles inside the heme P-ring vary only moderately (or slightly) with a change of multiplicity and upon ionization. As a rule, deformations do not exceed few hundredths of angstrom and few degrees, respectively. Geometric parameters of external carboxymethyl, vinyl, and methyl groups also do not change significantly. As expected, the Fe–N distance appears to be most sensitive toward the multiplicity and elongates from 1.98–2.00 Å for low- and middle-spin states to 2.05–2.07 Å for high-spin states. This elongation, typical for many metalloporphyrins, is related to the occupancy of the $d_{x^2-y^2}$-AO of the Fe atom (empty in low- and middle-spin and occupied in high-spin states) and its participation (or non-participation) in the donor–acceptor bonding with lone pairs of four N atoms [9,10]. The effect of occupation of the $d_{x^2-y^2}$-AO is also manifested in calculated frequencies and force constants of the vibrational modes with significant contributions from the Fe atom motions in the ring plane and perpendicular to it. Strictly speaking, in the lowest-frequency vibrations, the motions of the central atom are coupled with P-ring deformations, and so we discuss only the modes in these two ranges where the contributions of the Fe shifts, perpendicular (150–200 cm^{-1}) and in-plane (270–360 cm^{-1}), are most significant. The analysis shows that the low-limit values in these intervals, ~150 and ~270 cm^{-1}, correspond to high-spin states, while the upper-limit values, ~200 and ~360 cm^{-1}, correspond to low-spin states, in accord with the shortening of the R(Fe–N) distance from high-spin to low-spin states.

According to the results of vibrational frequency calculations, all the systems under discussion have 10 (or more) very low frequencies in the range of 10–100 cm^{-1}, which correspond to non-rigid (large-amplitude) vibrations of

the outside groups around single C–C and C–O bonds and to non-planar deformations of the P-ring. Obviously, many of these low-lying vibrational levels should be occupied at ambient temperatures, and the 'effective' structure, averaged upon all the occupied levels, can differ from the equilibrium one. The concept of 'static' geometry with fixed coordinates of atoms is not fully adequate for these species, and dynamic concepts are necessary for description of conformations and mutual orientation of periphery chains relative to the P-ring (see also [22]).

3.2. Fragments of heme and hemin$^+$ and fragmentation energies

As seen in Table 1, in the neutral product $FeC_{32}H_{29}N_4O_2$ (**2**) arising from the first step of heme fragmentation (elimination of a H_2CCO_2H-group), all three lowest multiplets, doublet, quartet and sextet, are very close in energy (within 0.2 eV). According to the calculated spin density distribution, both in the quartet and sextet states, one spin is delocalized in the P-ring and the Fe atom has two and four unpaired electrons, respectively. In the ion $FeC_{32}H_{29}N_4O_2^+$ (**2**$^+$), the lowest triplet and quintet are also very close to each other. In both states all unpaired electrons, two ($\rho(Fe) = 1.98$) in the doublet and four ($\rho(Fe) = 3.74$) in quartet, are localized on the Fe atom, and upon ionization of $FeC_{32}H_{29}N_4O_2$ (**2**), an electron is detached from the P-ring, but not from the central atom, as was the case upon ionization of heme (see above).

In the second neutral product $FeC_{30}H_{26}N_4$ (**3**) (without two H_2CCO_2H-groups), three lowest in energy multiplets, triplet, quintet and septet, form a close group within $\sim$ 0.2 eV, while the singlet lies $\sim$1.5 eV higher. The calculated spin-densities indicate that the Fe atom has two unpaired electrons in the triplet and quintet (ρ(Fe) is close to 2.00 in both states) and four spins in the septet ($\rho(Fe) \approx 3.75$), while the P-ring preserves two parallel spins in the quintet and septet. In the ion $FeC_{30}H_{26}N_4^+$ (**3**$^+$), spin distribution is more complicated; the quartet state is most favorable, and the doublet and the sextet lie $\sim$0.6 and $\sim$1.1 eV higher in energy, respectively. In the sextet, the Fe atom has four unpaired electrons ($\rho(Fe) \approx 3.75$), and in the ground quartet one spin is about equally shared between Fe and the P-ring. Certainly, the discussion of spin distribution in terms of spin-densities, which are calculated within the Mulliken population analysis, is approximate. Nevertheless, it is worth mentioning that most of the ρ values, calculated by us using various basis sets (Gen, 6-31G*, and 6-311++G**), vary only slightly with the basis set expansion and seem to be reasonable at least for high- and middle-spin states. The situation can be more complicated for low-spin states where multi-reference wave functions are necessary for adequate description and where single-determinant B3LYP calculations can provide only a semi-quantitative or qualitative picture.

As shown in Table 3, upon the fragmentation of heme and hemin$^+$, like upon heme ionization (see above), the bond length alteration in the P-ring moderately increases, usually within few hundredths of Å. The most significant elongations by 0.05–0.07 Å can be seen for the outer bonds of pyrrole rings. Like in heme and hemin$^+$, the Fe atom in their fragments remains located close to the center of the NNNN core, R(Fe–N) distances are shortened from the high-spin to the middle- and low-spin states by 0.06–0.08 Å in the cases where spin redistributions are localized inside the 3d-shell of the metal, according to the participation of the $3d_{x^2-y^2}$-AO in donor–acceptor bonding.

Calculated adiabatic ionization potentials of $FeC_{32}H_{29}N_4O_2$ and $FeC_{30}H_{26}N_4$ are close to each other, 5.81 and 5.73 eV, respectively, with ZPE corrections included, and decrease by 0.6 eV as compared to that for the heme. Dipole moments of the neutral species decrease monotonically with a decrease of multiplicity and the number of carboxymethyl groups. On the other hand, Mulliken's effective charge Z(Fe) on the metal atom vary in a narrow range from +0.90 to +1.28 e for all the systems and states under consideration, thus indicating that in contrast to ionization, multiplicity change and elimination of carboxymethyl groups in the heme and its ion are not accompanied by strong relaxation of valence MOs and electron density redistribution between the metal ion and the P-ring.

Fig. 4 shows the result of CID measurements for the dissociation of the first and the second carboxymethyl groups from the hemin$^+$ ion. The dissociation fractions are initially zero but increase nearly exponentially with E_{CM} as the collision energies reach 1.9 ± 0.2 and 2.4 ± 0.3 eV, respectively. The first dissociation energy measured is in reasonable agreement with the value $D_1^+(CMe) = 2.5 \pm 0.3$ eV reported in [5], but the second dissociation energy D_2^+, which is $\sim$0.5 eV higher than D_1^+, appears to be in contradiction with the estimate $D_2^+ \ll D_1^+$ suggested by Nonose et al. [5]. The determination of D_3 and higher becomes impractical because of the multiple CID products resulting from different dissociation channels (Fig. 3), which hinders a confident estimation of the total product abundance. However, the relative bond strength of the methyl and vinyl groups can still be determined by tandem mass measurements.

Fig. 3 depicts the CID fragment pattern of the isolated [heme–CH_2COOH]$^+$. In comparison with the fragments obtained by using photoexcitation (Fig. 2), only two peaks remain in each four groups (as discussed previously) with major peaks located at m/z 498, 483, 468, and 453. Obviously, this result shows a significant reduction of the fragmentation product, implying that the fragmentation of heme$^+$, either by CID or by photoexcitation, actually involve several dissociation channels. In this measurement, the ion with m/z 498 is the loss of second carboxymethyl group, whereas the rest of major fragments at 483, 468, and 453 are all differ by 15 amu, corresponding to the loss of three methyl side chains. Interestingly, there is no vinyl fragment observed in the entire energy range, implying that the dissociation of vinyl group requires considerably higher energy than that for the methyl groups. On the basis of this

result, we are able to predict that the relative bond strength of the side chains follows the order of CMe <Me < Vi.

The calculated (at the B3LYP/6-311++G** + ZPE level) elimination energies of the carboxymethyl groups, $D_1^+(\mathrm{CMe}) \approx 1.80$ eV and $D_2^+(\mathrm{CMe}) \approx 2.40$ eV, agree remarkably well with our experimental values (1.9 and 2.4 eV), supporting the observation that the second dissociation energy is higher than the first one by ~0.5 eV. After elimination of each of the CMe group, the ordinary single C_{16}–C_{28} and C_{18}–C_{29} bonds adjacent to the C_{28}–C_{58} and C_{29}–C_{44} bond which are cleaved, are shortened from 1.50 Å in $FeC_{34}H_{32}N_4O_4^+$ to 1.35–1.38 Å in $FeC_{32}H_{29}N_4O_2^+$ and $FeC_{30}H_{26}N_4^+$ (see Table 3), and their overlap populations increase almost by 2 times, thus implying transformation of the exterior C_{16}–C_{28} and C_{18}–C_{29} bonds into double bonds upon the CMe cleavage process. (In Table 3, only lengths of C_{16}–C_{28} and C_{28}–C_{58} bonds are given; the distances in C_{18}–C_{29} and C_{29}–C_{44} practically coincide (within few thousands of Å) with those of their counterparts and are not presented here.)

The situation is similar for fragmentation energies of the neutral heme molecule where the calculated values of D_1^0(CMe) and D_2^0(CMe) lie within a rather narrow range of 2.5–2.7 eV. For heme and hemin$^+$, D_1^0 is slightly lower than D_2^0 but is ~0.9 eV higher than D_1^+, while D_2^0 and D_2^+ are close to each other. Here, the $R(C_{16}$–$C_{28})$ and $R(C_{18}$–$C_{29})$ distances also shorten from 1.50 Å for $FeC_{34}H_{32}N_4O_4$ to 1.35–1.36 Å for $FeC_{32}H_{29}N_4O_2$ and $FeC_{30}H_{26}N_4$ due to a double-bond formation (Table 3).

Our calculations of further fragmentation products of the heme and its cation with sequential elimination of remaining peripheral methyl (Me) and vinyl (Vi) groups carried out at the same B3LYP/6-311++G** level (they will be described in detail in our future publication [23]) show that the fragmentation energies for the loss of methyl, D_i(Me), and vinyl, D_i(Vi), groups related to a cleavage of single C–C bonds lie in the range of 4.2–5.2 eV and are nearly two times higher than D_1^+(CMe) and D_2^+(CMe). This can be attributed to the fact that, as discussed above, upon elimination of carboxymethyl groups, the single C_{16}–C_{28} and C_{18}–C_{29} bonds turn into double bonds. The energy expenses for the loss of both first and second CMe-groups are compensated to a similar extent by the formation of new C_{16}–C_{28} and C_{18}–C_{29} π-bonds. Therefore, the suggestion made in [5] that D_2^+(CMe) should be much lower than D_1^+(CMe) seems to be questionable.

4. Summary

Density functional B3LYP calculations have been carried out for heme, hemin$^+$ and products of their fragmentation with consequent cleavage of two carboxymethyl groups to investigate their geometric and electronic structures, vibrational frequencies, relative energies of electronic states with different spin multiplicities, and fragmentation energies. The calculated fragmentation energies are in excellent agreement with their experimental values measured by collision-induced dissociation in an ion cyclotron resonance cell.

Acknowledgments

The experimental part of this work was supported by grants from Academia Sinica and the National Science Council (Grant No. NSC 92-3112-B-001-012-Y) of Taiwan. We thank S. Sabu and Dr. C.-C. Han for setting up the FT-ICR mass spectrometer and insightful discussions. O.P.C. and N.M.K. thank Prof. S.H. Lin for invitation to visit the Institute of Atomic and Molecular Sciences, Academia Sinica.

References

[1] K. Kadish, K.M. Smith, R. Guilard (Eds.), The Porphyrin Handbook, Academic Press, San Diego, 2000.
[2] K. Kalyanasundaram, Photochemistry of Polypyridine and Porphyrin Complexes, Academic Press, London, 1992.
[3] R.B. Cole (Ed.), Electrospray Ionization Mass Spectrometry, Wiley, New York, 1997.
[4] E. Antonini, M. Brunori, Hemoglobin and Myoglobin in their Reactions with Ligands, North-Holland, Amsterdam, 1971.
[5] S. Nonose, H. Tanaka, N. Okai, T. Shibakusa, K. Fuke, Eur. Phys. J. D 20 (2002) 619.
[6] M. Rivera, G.A. Caignan, A.V. Astashkin, A.M. Raitsimring, T.K. Shokhireva, F.A. Walker, J. Am. Chem. Soc. 124 (2002) 6077.
[7] S. Shaik, M. Filatov, D. Schroder, H. Schwarz, Chem.-Eur. J. 4 (1998) 193.
[8] P.M. Kozlowski, T.G. Spiro, A. Berces, M.Z. Zgierski, J. Phys. Chem. B 102 (1998) 2603.
[9] J.M. Ugalde, B. Dunietz, A. Dreuw, M. Head-Gordon, R.J. Boyd, J. Phys. Chem. A 108 (2004) 4653.
[10] A. Ghosh, in: K. Kadish, K.M. Smith, R. Guilard (Eds.), The Porphyrin Handbook, vol. 7, Academic Press, San Diego, 2000 (Section 47).
[11] C. Lecomte, M.-M. Rohmer, M. Benard, in: K. Kadish, K.M. Smith, R. Guilard (Eds.), The Porphyrin Handbook, vol. 7, Academic Press, San Diego, 2000, Sec. 48.
[12] Y.-S. Wang, S.-J. Wei, C.-C. Kau, S. Sabu, Y.T. Lee, C.-C. Han, H.-C. Chang, Z.H.J. Zhang (in preparation).
[13] P.J. Stephens, F.J. Devlin, C.F. Chabalowski, M.J. Frisch, J. Phys. Chem. 98 (1994) 11623.
[14] A.D. Becke, J. Chem. Phys. 98 (1993) 5648.
[15] C. Lee, W. Yang, R.G. Parr, Phys. Rev. B 37 (1988) 785.
[16] M.J. Frisch et al., Gaussian 03, Revision B.03, Gaussian, Pittsburgh, PA, 2003.
[17] K.R. Babu, D.J. Douglas, Biochem. 39 (2000) 14702.
[18] A.G. Marshall, C.L. Hendrickson, G.S. Jackson, Mass Spectrom. Rev. 17 (1998) 1.
[19] S. Pagola, P.W. Stephens, D.S. Bohle, A.D. Kosar, S.K. Madsen, Nature 404 (2000) 307.
[20] J.P. Collman, J.L. Hoard, N. Kim, G. Lang, C.A. Reed, J. Am. Chem. Soc. 97 (1975) 2676.
[21] C.A. Reed, T. Mashiko, W.R. Sheidt, K. Spartalian, G. Lang, J. Am. Chem. Soc. 102 (1980) 2302.
[22] O.P. Charkin, N.M. Klimenko, T.P. Nguyen, D.O. Charkin, Y.-S. Wang, S.-C. Wei, H.-C. Chang, S.H. Lin, Russ. J. Inorg. Chem. (Engl. Transl.) 50 (2005) 1398.
[23] O.P. Charkin, N.M. Klimenko, T.P. Nguyen, D.O. Charkin, A.M. Mebel, Y.-S. Wang, S.-C. Wei, H.-C. Chang, S.H. Lin, Russ. J. Inorg. Chem. (Engl. Transl.) 51 (2006) #1 (in press).